Time of Arrival Distribution Differences in Neutrinos from Kaon vs. Pion Decay and Timing Cut Development: DRAFT 1

Melanie Novak
Bucknell University

Jocelyn Monroe
Columbia University

Steve Brice
Fermi National Accelerator Laboratory

August 8, 2001

Introduction

The intrinsic ν_e content of the MiniBooNE ν_μ beam from sources other than ν_μ oscillations is the primary background to the oscillation signal. This content is on the order of 1%. The ν_e contamination in the beam is due to kaon and muon decays. In this memo we investigate the possibility of making a timing cut to reduce the background due to kaon decays.

Kaon decay modes often produce electron neutrinos. Approximately 5% of K^+ decays and 40% of K_L^0 decays produce ν_e. Our goal is to separate the ν_e from kaon decays from the possible ν_e from ν_μ oscillations.

The basic scheme is as follows: kaons and pions have different masses, and are produced at different energies in our beam. These differences lead to the kaons and pions in our beam having different speeds and different lifetimes. Taking this into consideration, we find that neutrinos from kaon decay will take longer to reach our detector than neutrinos from pion decay. Here we present a preliminary analysis of the differences in time-of-interaction distributions in the detector of neutrinos from pion decays vs. neutrinos from kaon decays. Using an analytical model developed by Steve Brice to describe the time-of-interaction distribution for ν_μ from π^+ decay,

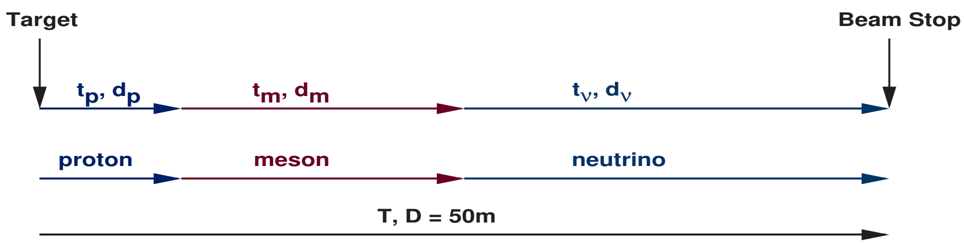

Figure 1: The simple analytical model for the neutrino time of arrival at the beam stop.

we separate $K \rightarrow \nu_e + X$ from $\pi^+ \rightarrow \mu^+ + \nu_\mu$, and demonstrate a maximum efficiency of $\sim$ 40% for rejecting ν_e from kaon decays.

1 A Simplified Analytical Model of $\pi \rightarrow \nu_\mu + X$ and $K \rightarrow \nu_e + X$ in the MiniBooNE Decay Pipe

The analytical model assumes that all pions, kaons, and their decay products are produced along a straight line towards the detector, see Figure 1. It assumes perfect detector resolution in both energy and time. It also assumes that the proton bunch incident on the MiniBooNE target is a delta function in time and energy, with all protons having a total energy of 8.9 GeV, incident at the same instant in time.

The time of arrival at the beam stop ($\Delta\ t$) is of primary importance to this study. It is defined as:

$$\Delta t \ = \ t_p + t_m + t_\nu - T; \tag{1}$$

where:

$$t_m \ = \ d_m/\beta_m; \quad t_p \ = \ d_p/\beta_p; \quad t_\nu \ = \ T - d_m - d_p. \tag{2}$$

For an 8.9 GeV proton, $\beta \simeq 1$, so $t_p \simeq d_p$. The interaction length in the beryllium MiniBooNE target is approximately 10 cm, which is much less than the 50 m length of the decay pipe. Therefore we neglect the time of flight for the proton, t_p, and:

$$\Delta t \ = \ t_m(1 - \beta_m). \tag{3}$$

The probability to find a meson as a function of time (or distance along the decay pipe), which derives from the basic decay law $N = N_0 e^{(-t/\tau)}$, is:

$$P(t_m)dt_m = 1/(\gamma_m \tau_m) e^{-t_m/(\gamma_m \tau_m)} dt_m. \qquad (4)$$

We include a Heaviside function to ensure that the meson decays before the beam stop, substitute Δt for t_m, and normalize to one when integrated over Δt. Then:

$$P(\Delta t)d\Delta t = \frac{e^{-\Delta t/[(1-\beta_m)\gamma_m \tau_m]} \Theta[D(1/\beta_m - 1) - \Delta t] d\Delta t}{(1-\beta_m)\gamma_m \tau_m [1 - e^{-D/(\beta_m \gamma_m \tau_m)}]}. \qquad (5)$$

Using simple kinematics we solve for the maximum neutrino energy and maximum Δt for neutrinos from pion decay:

$$\begin{aligned} E_{\nu,max} &= \frac{1}{2}(M_\pi^2 - M_\mu^2)/(E_\pi - p_\pi); \\ \Delta t_{\nu_\mu,max} &= 2D/[(33.6 E_\nu)^2 - 1]. \end{aligned} \qquad (6)$$

Plotting the maximum $\Delta t_{\nu_\mu,max}$ curve for neutrinos from pion decay with Monte Carlo data reconstructed in the detector shows the promise of using this function as a cut to reduce background from kaon decays, see Figure 2. We place two cuts on the neutrinos at the beam stop. The first is a flat energy cut, E_{cut}, eliminating all neutrinos with energies greater than 2.5 GeV. The second cut eliminates all neutrinos that lie above the $\Delta t_{\nu_\mu,max}$ curve for neutrinos from pion decay, Δt_{cut}. These cuts eliminate much of the ν_e background from kaon decay without losing a significant portion of the ν_μ beam. For the number of particles failing cuts see Table 1. For the timing and energy distributions for the Monte Carlo data before and after cuts are applied, see Figures 3 and 4. Here we use the assumption of a delta function proton bunch (in both energy and time) incident on the target.

cuts	$\pi^\pm \to \nu_\mu + X$	$K^\pm \to \nu_e + X$	$K^0{}_L \to \nu_e + X$
total uncut	290355	308	144
$E < 2.5$ GeV	646	96	34
$\Delta t < \Delta t_{\nu_\mu,max}$	2187	162	68
E_{cut} and Δt_{cut}	2833	258	102
Rejection η	1.0%	84%	71%

Table 1: Number of ν_μ and ν_e cut by (i) $E < 2.5$ GeV, (ii) $\Delta t < \Delta t_{\nu_\mu,max}$, and (i) + (ii)

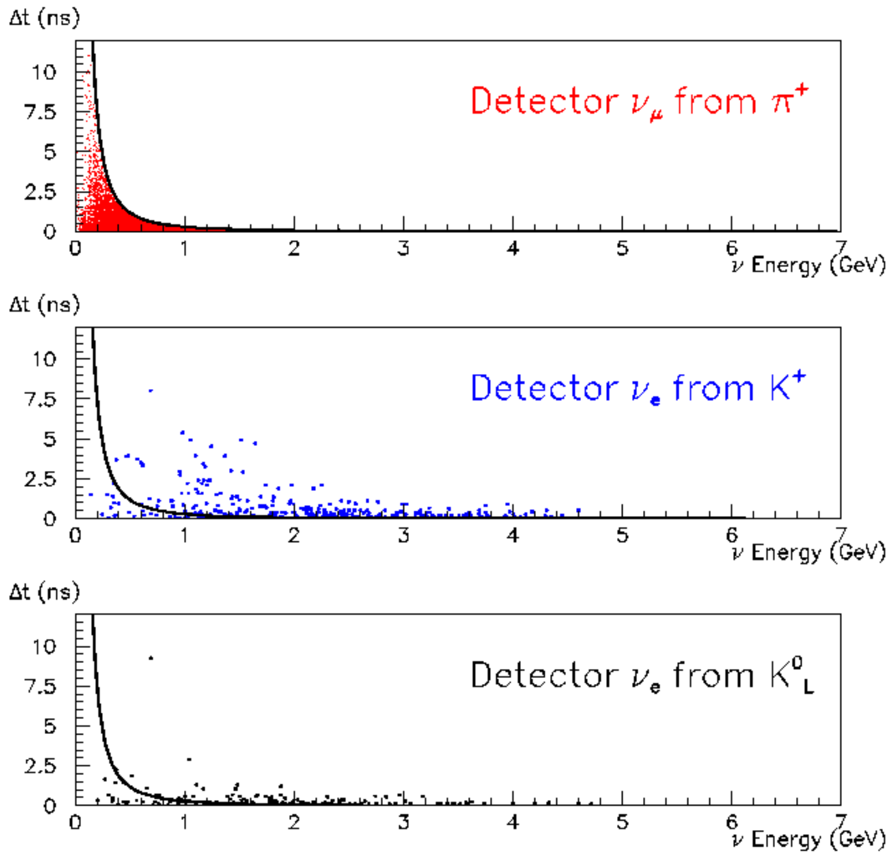

Figure 2: Reconstructed Energy vs. Time of Reconstruction in the detector for unsmeared monte carlo data, with the analytic maximum $\Delta t_{\nu_\mu,max}$ curve for neutrinos from pion decay overlaid. We assume a delta function proton bunch (in both energy and time) incident on the target.

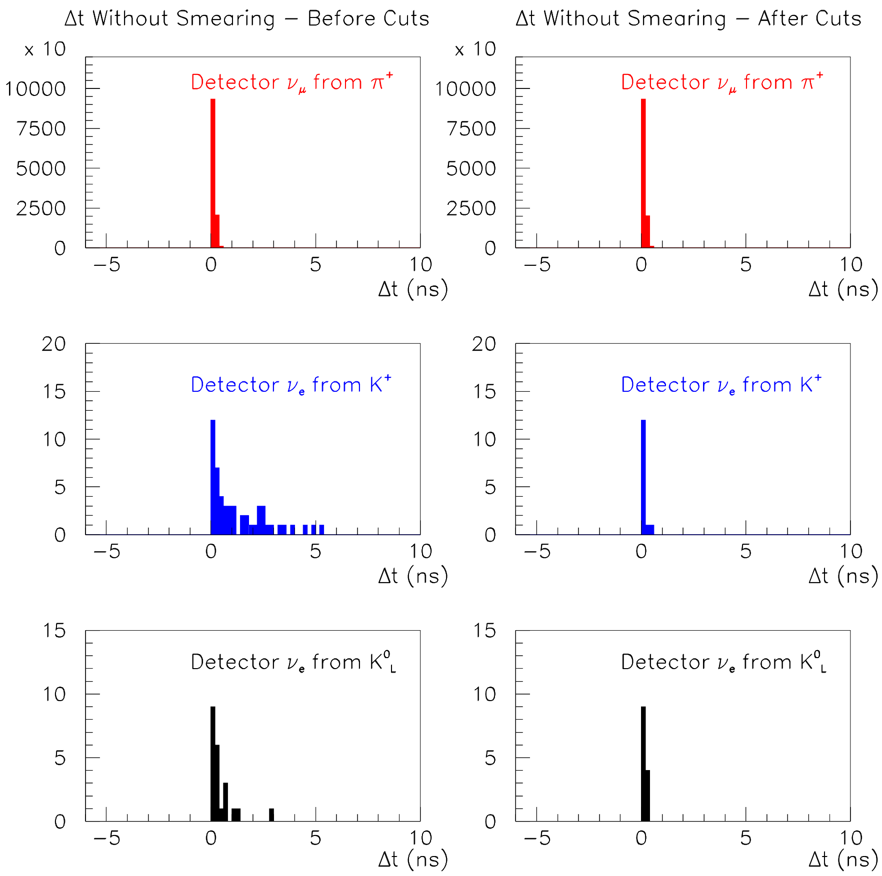

Figure 3: Time of reconstruction distributions for unsmeared Monte Carlo data before and after cuts are applied. Cuts: (i) $E < 2.5\ GeV$ and (ii) $\Delta t < \Delta t_{\nu_\mu,max}$. Top: ν_μ from π^+ decay, Middle: ν_e from K^+ decay, Bottom: ν_e from $K_L{}^0$ decay. We use the assumption of a delta function proton bunch (in both energy and time) incident on the target.

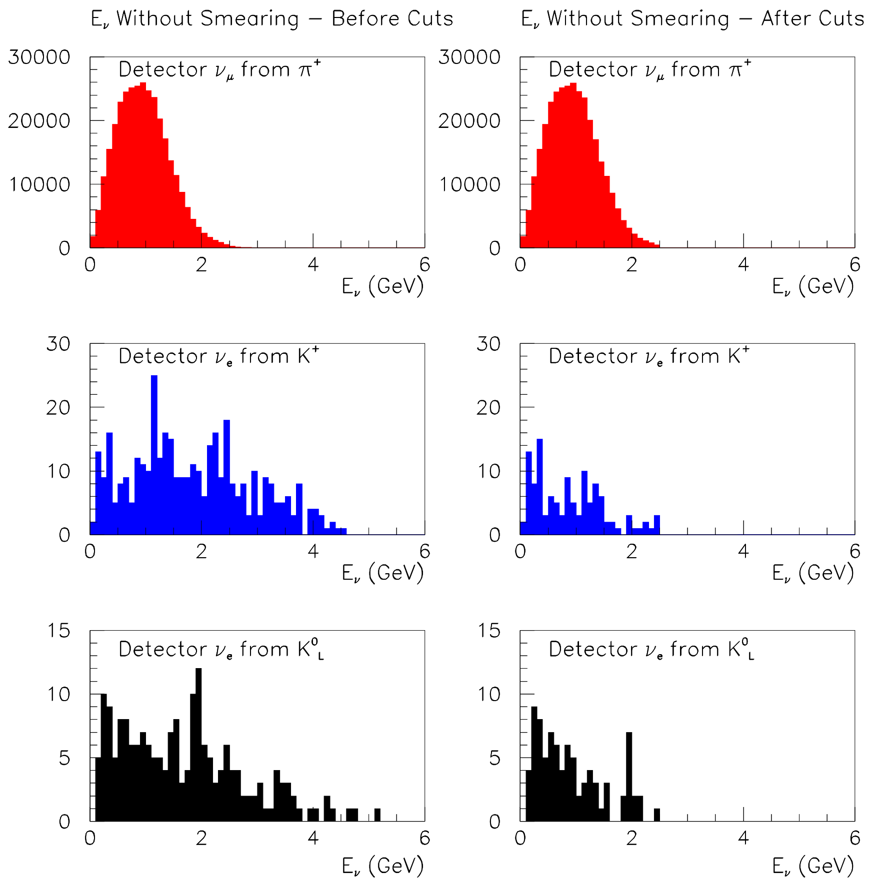

Figure 4: Reconstructed Energy distributions for unsmeared Monte Carlo data before and after cuts are applied. Cuts: (i) $E < 2.5\ GeV$ and (ii) $\Delta t < \Delta t_{\nu_\mu,max}$. Top: ν_μ from π^+ decay, Middle: ν_e from K^+ decay, Bottom: ν_e from ${K_L}^0$ decay. We use the assumption of a delta function proton bunch (in both energy and time) incident on the target.

2 Corrections to the Simplified Model

The proton bunch is not a delta function in time, nor do we have perfect detector resolution, so we smear the reconstructed energy and time for neutrinos in the detector. Our smearing in energy comes solely from our finite detector resolution. We incorporate this into the analysis by adding gaussian smearing in the reconstructed energy with a width ($\sigma_E = \Delta E/E$) of 0.1. Smearing in the time-of-interaction distribution comes from two sources; the detector vertex resolution, which we call the fitting width (σ_{vertex}), and the width of the proton bunch on the target in time, which we call the bucket width (σ_{proton}). We add σ_{vertex} and σ_{proton} in quadrature to get the total gaussian smearing width in time (σ_t):

$$\sigma_t \;=\; \sqrt{(bucketwidth)^2 + (fittingwidth)^2} \;=\; \sqrt{\sigma^2_{proton} + \sigma^2_{vertex}}. \qquad (7)$$

2.1 Gaussian Smearing

In Figure 5 we plot energy smeared with $\sigma_E = 0.1$, and time smeared with $\sigma_t = 1.97\,ns$, where the bucket width $= 1.75\,ns$ and the fitting width $= 0.9\;ns$. The assumptions that affect our choices of smearing parameters are as follows: one, that the 95% width of the proton bunch in time is 7 ns, which may be overly pessimistic; two, that the vertex reconstruction uncertainty (fitting width) is 0.9 ns; and three, that the energy reconstruction uncertainty is of order 10%. The timing and energy distributions for the gaussian smeared Monte Carlo before and after cuts are shown in Figures 6 and 7.

Due to the smearing in energy and time, our $\Delta t_{\nu_\mu,max}$ curve cuts out more of our neutrinos from pion decay than we would like. We redefine our Δt cut by shifting the $\Delta t_{\nu_\mu,max}$ curve up in time by 1.5 ns. The new Δt cut is:

$$\Delta t' \;<\; 1.5 + \Delta t_{\nu_\mu,max} \qquad (8)$$

The purpose of the shift is to cut a minimum number of ν_μ from pion decay, while eliminating the maximum possible number of ν_e from kaon decays. The shift will be optimized at the end of our analysis.

With the same $E_\nu < 2.5\;GeV$ energy cut as before, and the shifted $\Delta t_{\nu_\mu,max}$ cut: $\Delta t < 1.5 + \Delta t_{\nu_\mu,max}$, we cut 51% of ν_e from K^+ decays and 42% of ν_e from K^0_L decays, while losing 17% of neutrinos from π^+ decay, see Table 2.

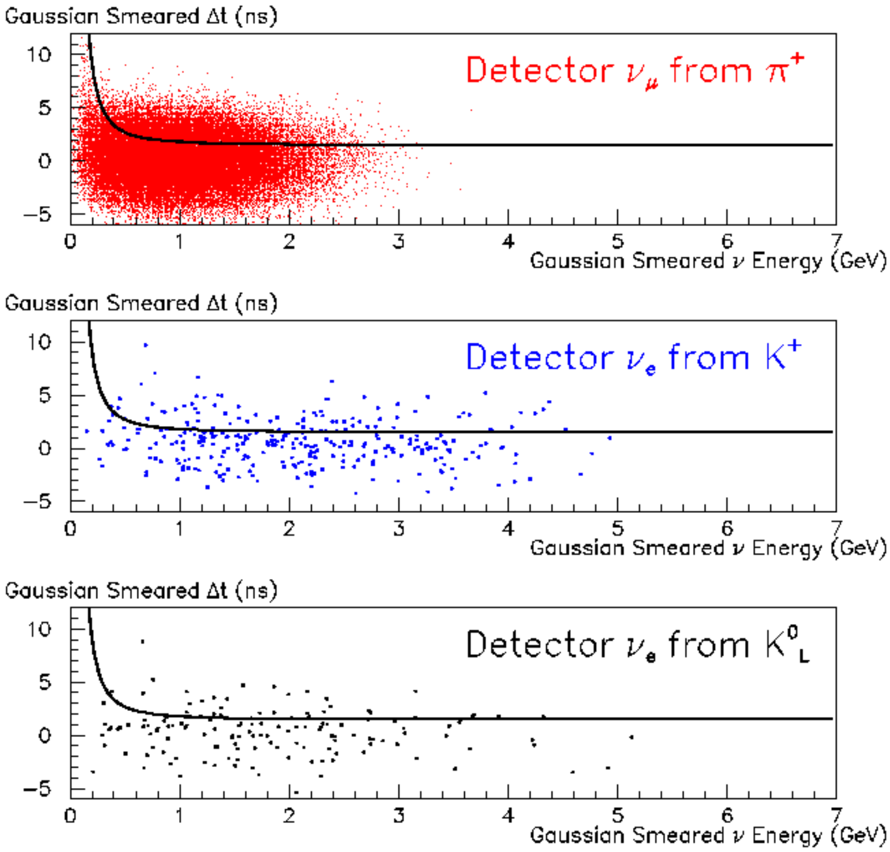

Figure 5: Reconstructed Energy vs. Time of Reconstruction in the detector for gaussian smeared monte carlo data. The black curve represents the timing cut $\Delta t' \; < \; 1.5 + \Delta t_{\nu_\mu,max}$. All particles that lie above this curve are cut. Top: ν_μ from π^+ decay, Middle: ν_e from K^+ decay, Bottom: ν_e from ${K_L}^0$ decay. The reconstructed energy is smeared with a gaussian of width $\sigma_E = \Delta E/E = 0.1$. The time of reconstruction is smeared with a gaussian of width $\sigma_t = \sqrt{{\sigma_{proton}}^2 + {\sigma_{vertex}}^2} = 1.97\ ns$ where $\sigma_{proton} \; = \; 1.75\ ns$ and $\sigma_{vertex} = 0.9\ ns$.

cuts	$\pi^{\pm} \to \nu_\mu + X$	$K^{\pm} \to \nu_e + X$	${K^0}_L \to \nu_e + X$
total uncut	290355	308	144
$E < 2.5\ GeV$	1107	100	32
$\Delta t' < 1.5 + \Delta t_{\nu_\mu,max}$	49700	57	29
E_{cut} and $\Delta t'_{cut}$	50807	157	61
Rejection η	17%	51%	42%

Table 2: Number of ν_μ and ν_e Cut by (i) $E < 2.5\,GeV$, (ii) $\Delta t' < 1.5 + \Delta t_{\nu_\mu,max}$, and (i) + (ii)

The numbers in Table 2 for the cut percentages may be overly pessimistic, owing to our assumptions about the beam. First of all, we assumed a bucket width of 7 ns; but the width in time of the proton bunches will probably be closer to 5 ns, in which case the timing cut we apply will cut fewer ν_μ from pion decays, while still rejecting a significant portion of ν_e from kaon decays. Figure 8 shows the dependance of the percentage of neutrinos cut on the bucket width for gaussian smearing in energy with $\sigma_E = 0.1$ and gaussian smearing in time with $\sigma_t = \sqrt{(bucketwidth)^2 + (0.9)^2}$. Further, we will show that the distribution in time of the proton bunch is more parabolic than gaussian, which will also improve our ratio of neutrinos from kaon decay cut to the neutrinos from pion decay cut.

2.2 Parabolic Smearing

Since the timing distribution of proton bunches incident on the target is actually parabolic in shape (see Figure 10) fewer particles will populate the tails than in the previously assumed gaussian distribution. If we smear the time-of-interaction distribution with a parabola of the form $y = 1 - x^2$, we find that the number of neutrinos from pion decay cut is reduced from 17% to 10% at a bucket width of 1.75 ns and a fitting width of 0.9 ns, while the removal of neutrinos from kaon decay remains fairly steady, see Figure 9. For this reason we conclude that using the more realistic parabolic smearing function improves the effectiveness of our timing cut.

3 Measurements of the Proton Beam Timing Distribution

With Bill Pellico, we took measurements of the proton beam at Long 7 in the Booster, using a Lecroy Digital Oscilloscope. The scope triggers off of the low-level RF and samples the integrated charge of the bunch on a

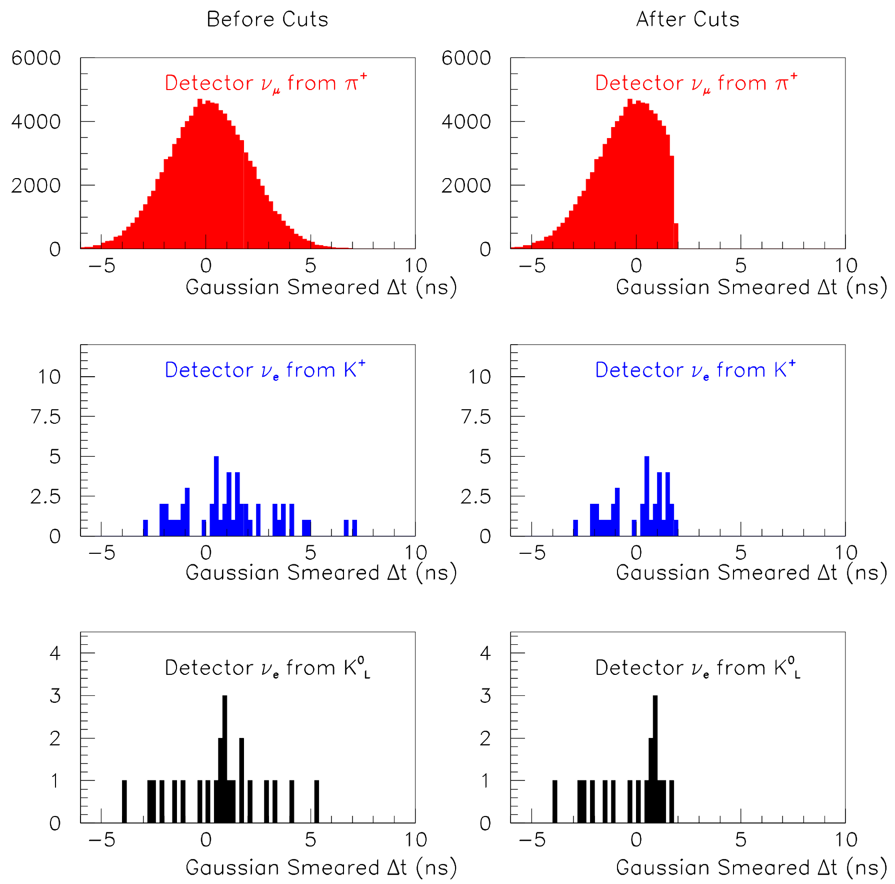

Figure 6: Time of reconstruction distribution for gaussian smeared Monte Carlo data before and after cuts are applied. Cuts: (i) $E < 2.5\ GeV$ and (ii) $\Delta t' < 1.5 + \Delta t_{\nu_\mu,max}$. Top: ν_μ from π^+ decay, Middle: ν_e from K^+ decay, Bottom: ν_e from $K_L{}^0$ decay. The time of reconstruction is smeared with a gaussian of width $\sigma_t = \sqrt{\sigma_{proton}{}^2 + \sigma_{vertex}{}^2} = 1.97\ ns$ where $\sigma_{proton} = 1.75\ ns$ and $\sigma_{vertex} = 0.9\ ns$. The reconstructed energy is smeared with a gaussian of width $\sigma_E = \Delta E/E = 0.1$.

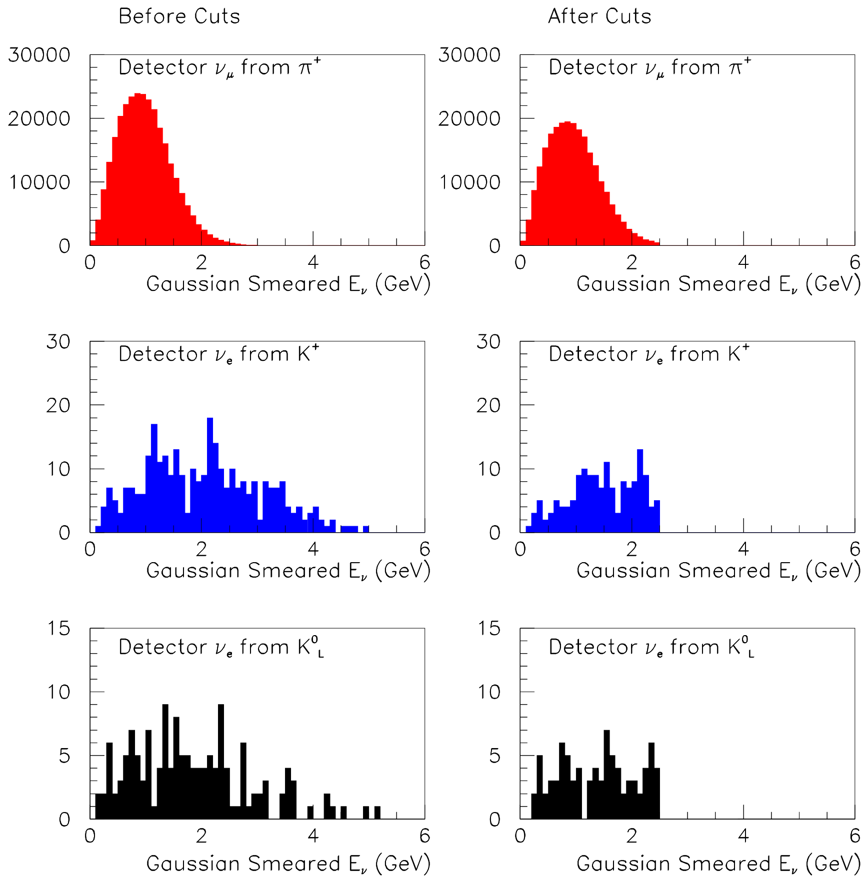

Figure 7: Reconstructed Energy distribution for gaussian smeared Monte Carlo data before and after cuts are applied. Cuts: (i) $E \ < 2.5 \ GeV$ and (ii) $\Delta t' \ < \ 1.5 + \Delta t_{\nu_\mu, max}$. Top: ν_μ from π^+ decay, Middle: ν_e from K^+ decay, Bottom: ν_e from $K_L{}^0$ decay. The time of reconstruction is smeared with a gaussian of width $\sigma_t = \sqrt{\sigma_{proton}{}^2 + \sigma_{vertex}{}^2} = 1.97 \ ns$ where $\sigma_{proton} = 1.75 \ ns$ and $\sigma_{vertex} = 0.9 \ ns$. The reconstructed energy is smeared with a gaussian of width $\sigma_E = \Delta E/E = 0.1$.

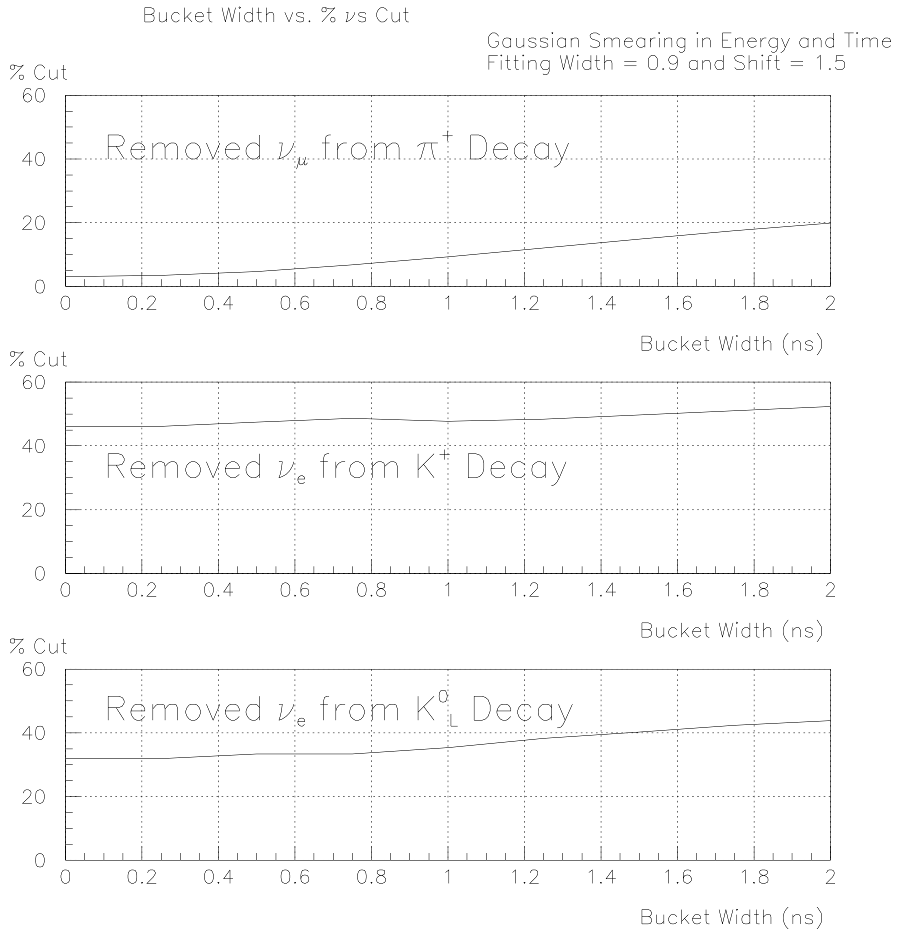

Figure 8: Percentage of neutrinos cut vs. Bucket width for gaussian smeared monte carlo reconstructed data. Cuts: (i) $E \ < 2.5\ GeV$ and (ii) $\Delta t' \ < \ 1.5 + \Delta t_{\nu_\mu,max}$. Top: ν_μ from π^+ decay, Middle: ν_e from K decay, Bottom: ν_e from ${K_L}^0$ decay. The reconstructed energy is smeared with a gaussian of width $\sigma_E = \Delta E/E = 0.1$. The time of reconstruction is smeared with a gaussian of width $\sigma_t \ = \ \sqrt{{\sigma_{proton}}^2 + {\sigma_{vertex}}^2}$, where σ_{proton} is the variable bucket width and $\sigma_{vertex} = 0.9\ ns$.

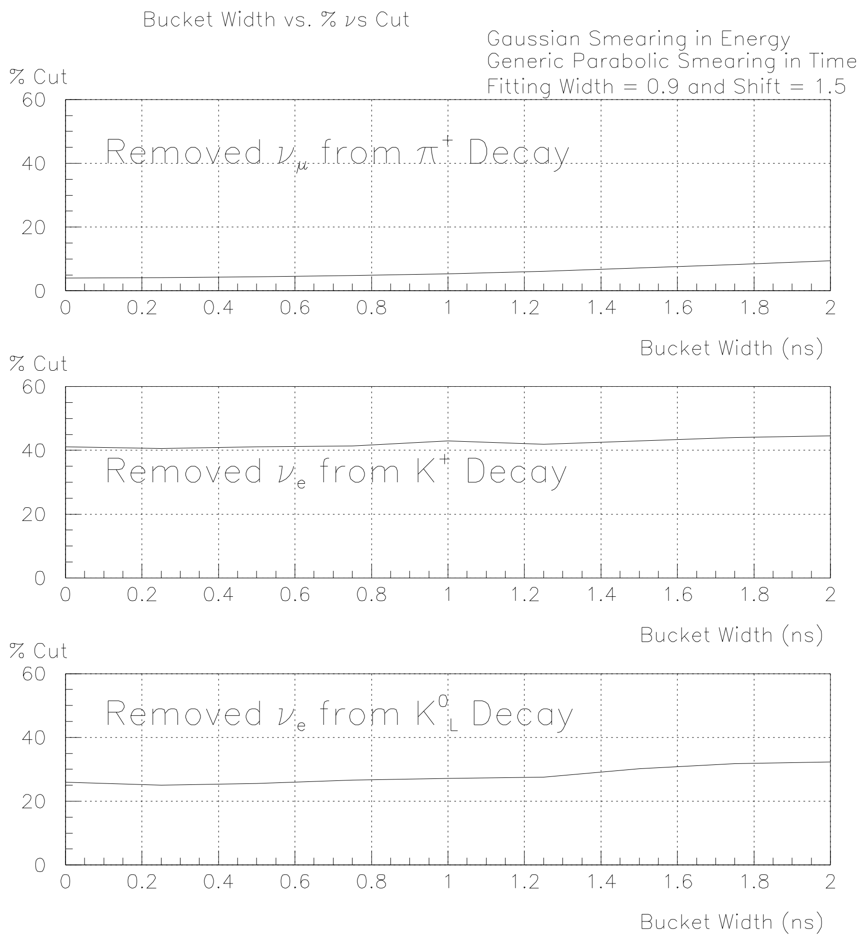

Figure 9: Percentage of neutrinos cut vs. Bucket width for parabolic smeared monte carlo reconstructed data. Cuts: (i) $E \; < \; 2.5 \; GeV$ and (ii) $\Delta t' \; < \; 1.5 + \Delta t_{\nu_\mu,max}$. Top: ν_μ from π^+ decay, Middle: ν_e from K^+ decay, Bottom: ν_e from ${K_L}^0$ decay. The reconstructed energy is smeared with a gaussian of width $\sigma_E = \Delta E/E = 0.1$. The time of reconstruction is smeared with a gaussian of width $\sigma_v ertex \; = \; 0.9 \; ns$ and a parabola of the form $y = 1 - x^2$, where the total area of the parabola is normalized to be the same as that of a gaussian of total width 7 ns, as is the case in the gaussian smeared timing distributions of the previous subsection.

resistive wall monitor with a frequency of 8 GHz. We took data on beam with a total energy of 8.9 GeV and 5.1×10^{12} protons per pulse, which are approximately the conditions for MiniBooNE running. Each pulse contains up to 84 bunches (determined by the 53 MHz RF frequency at the time extraction), and there are 15 pulses per second extracted from the booster. A sample data file of the amplitude of the integrated charge on the resistive wall monitor vs. time from the scope is shown in Figure 10.

The bunches have the interesting feature of a small pre-peak in amplitude, which is apparent in Figure 11. This could be an artifact of the measurement, since the scope was triggered off of the RF, and not the beam itself. An offset between the beam and the low-level RF could result in the behavior we observe. Or, this feature could be part of the actual beam structure.

We use data from 36 bunches, a total time sample of 0.68 μs, which we average together to make a representative fit to the timing distribution of a single bunch, see Figure 11. The procedure we use to average the bunches is as follows. We define the total time spread of the bunch to be the time of maximum amplitude $\pm$ 10 ns. We then subtract the time of the maximum amplitude from all points in the bunch, i.e. we set the time of maximum amplitude to zero. Since the scope triggers off of the low-level RF(which fixes the start time for the measurement), this procedure results in 20 measurements of the bunch amplitude vs. time, where the 20 time values are identical for all 36 bunches. We then average by summing the amplitudes that are greater than zero at equal times, and dividing by the number of measurements greater than zero at equal times.

To include the maximum possible time spread, the averaged bunch was doctored to reflect the full time spread of the bunch plus the pre-peak structure, see Figure 12. We also preserved the parabolic shape of the bunch (compare the data points of Figure 12 with those of Figure 10). A gaussian fit to the doctored bunch has a σ of 1.3 ns, which is 20% smaller than the 1.75 ns bucket width assumed earlier. However, the poor χ^2 of 69/D.O.F. reflects the parabolic rather than gaussian shape of the bunch, see Figure 12. Our doctored bunch may be an overly pessimistic estimate of the full time spread of the proton bunch on target. Further work will be done to understand the source of the pre-peak structure, and its implications for this analysis.

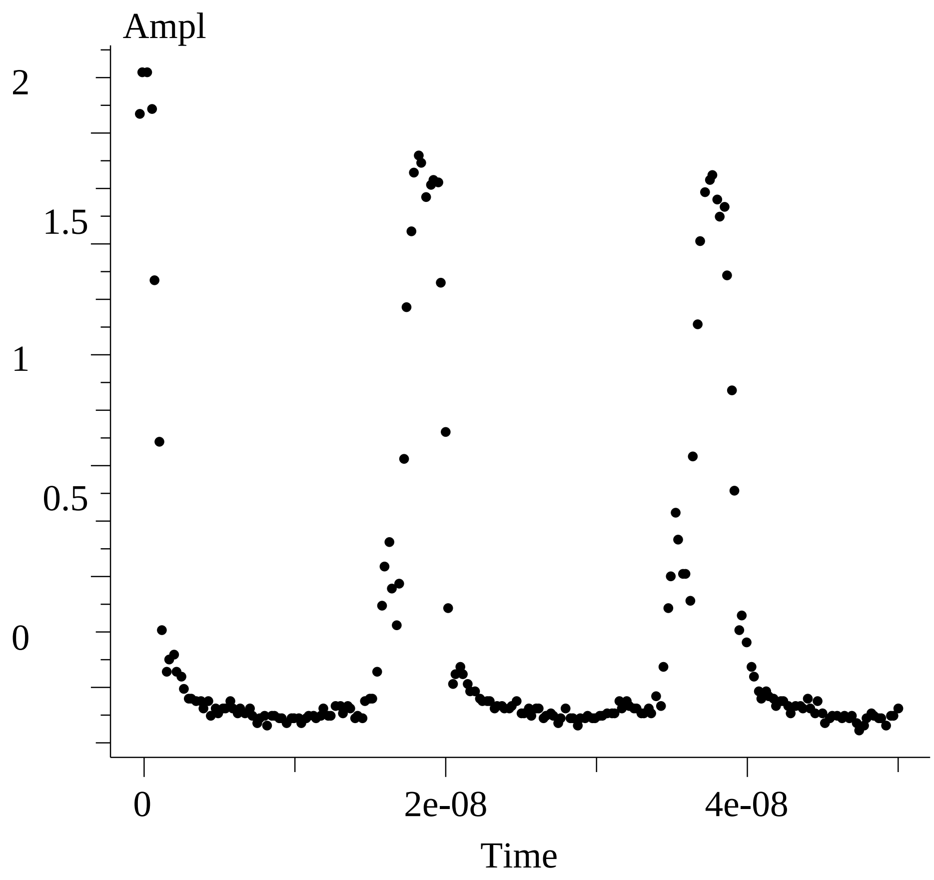

Figure 10: Sample measurement of the amplitude of integrated charge vs. time on a resistive wall monitor at Long 7 in the booster. Measurements were taken at a sample rate of 8 GHz when the proton beam had a total energy of 8.9 GeV and 5.1×10^{12} protons per pulse.

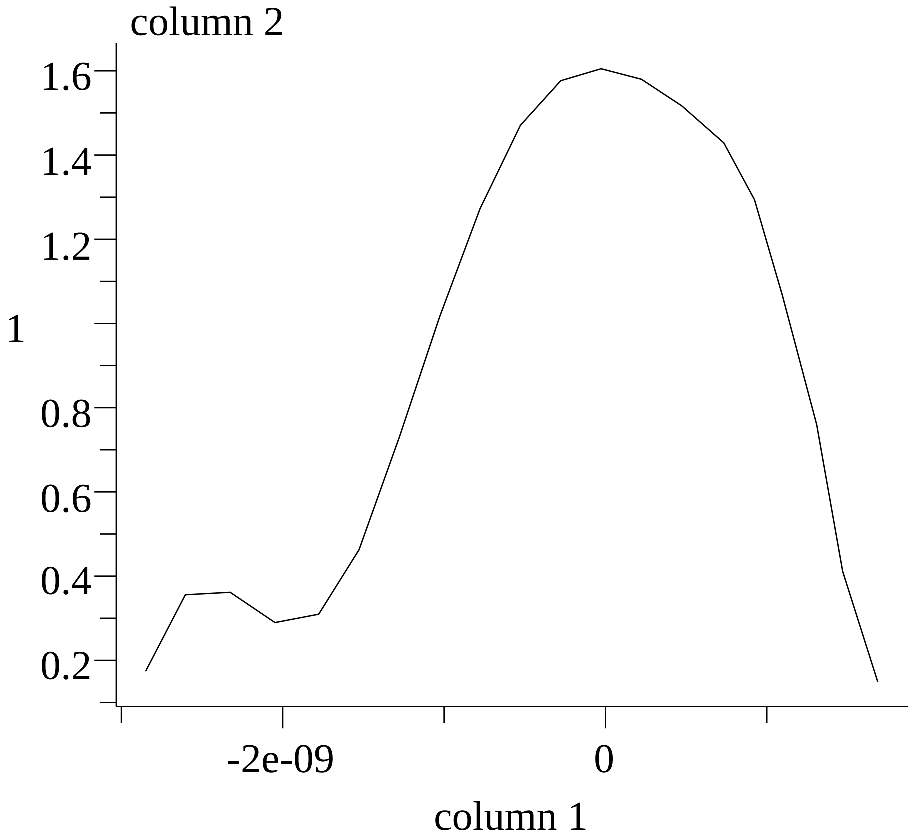

Figure 11: Average of 36 bunch measurements of the amplitude of integrated charge vs. time on a resistive wall monitor at Long 7 in the booster. Measurements were taken at a sample rate of 8 GHz when the proton beam had a total energy of 8.9 GeV and 5.1×10^{12} protons per pulse.

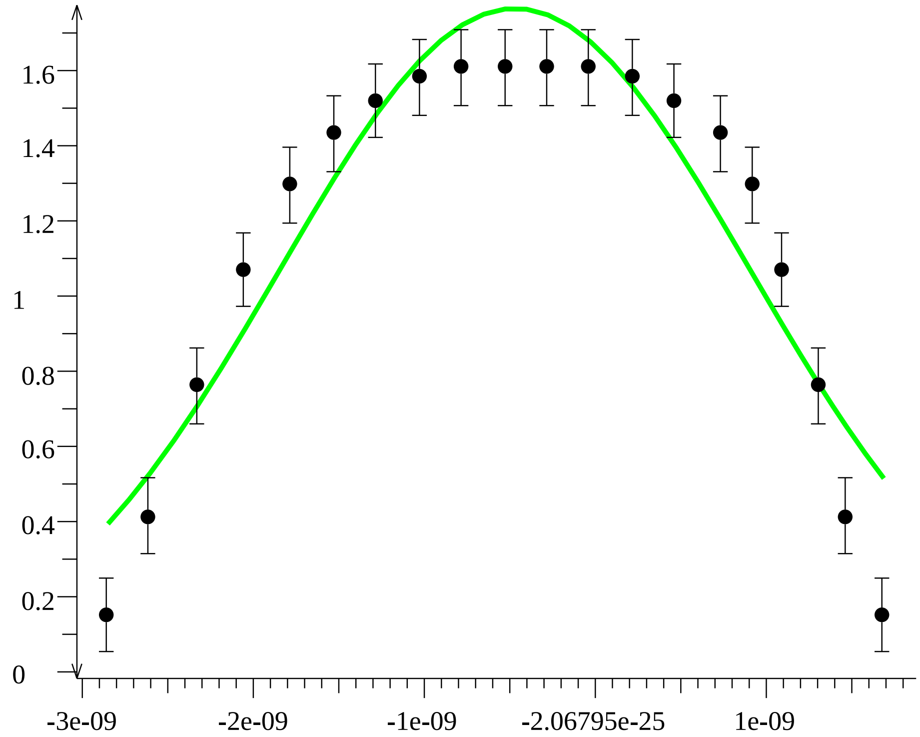

Figure 12: Average of 36 bunch measurements of the amplitude of integrated charge vs. time on a resistive wall monitor at Long 7 in the booster, doctored to include the maximum possible time spread (including the pre-peak structure) and to preserve the parabolic shape of the proton bunches. Measurements were taken at a sample rate of 8 GHz when the proton beam had a total energy of 8.9 GeV and 5.1×10^{12} protons per pulse. The smooth line is a gaussian fit to the doctored bunch, with $\sigma = 1.3\ ns$, and $\chi^2 = 69/D.O.F.$ The poor χ^2 reflects the parabolic rather than gaussian shape of the bunch.

3.1 Realistic Smearing

We smear the monte carlo reconstructed neutrinos in the detector according to a parabola with the height and width of the doctored bunch, where x is in nanoseconds, (see Figure 13):

$$y = 1.605 - 0.331x^2. \tag{9}$$

We find that the percentage of ν_e cut decreases, see Table 3. The timing and energy distributions before and after cuts for the Monte Carlo smeared with the parabolic function derived from the doctored bunch are shown in Figures 14 and 15.

cuts	$\pi^{\pm} \to \nu_\mu + X$	$K^{\pm} \to \nu_e + X$	$K^0{}_L \to \nu_e + X$
total uncut	290355	308	144
$E < 2.5\ GeV$	1107	100	32
$\Delta t' \ < \ 1.5 + \Delta t_{\nu_\mu,max}$	27204	62	25
E_{cut} and Δt_{cut}	28311	162	57
Rejection η	10%	53%	40%

Table 3: Number of ν_μ and ν_e Cut by (i) $E \ < 2.5\, GeV$, (ii) $\Delta t' \ < \ 1.5 + \Delta t_{\nu_\mu,max}$, and (i) + (ii)

3.2 Optimizing the $\Delta t_{\nu_\mu,max}$ Shift

Until now, we have used a shift of + 1.5 ns in the $\Delta t_{\nu_\mu,max}$ cut. The purpose of this shift is to improve the ratio of ν_e from kaon decays cut to ν_μ from pion decay cut. Figure 16 shows the shift vs. rejection efficiency for the monte carlo smeared according to a parabolic fit to the bunch data. The reconstructed energy is smeared with a gaussian of width $\sigma_E = \Delta E/E = 0.1$. The time of reconstruction is smeared with the parabolic function derived from the data: $y = 1.605 - 0.331^2$, see Figure 12, and a gaussian function of $\sigma \ = \ 0.9\ ns$ corresponding to the detector timing resolution. The optimal shift would maximize the percentage of neutrinos from pion decay kept and maximize the percentage of neutrinos from kaon decay rejected. In Figure 17 we plot the percent of neutrinos from kaon decay rejected vs. the percent of neutrinos from pion decay retained for shift values between zero and two nanoseconds. Depending on how much of the ν_μ beam it is acceptable to cut, the timing cuts developed here can have an efficiency of up to 73% in rejecting ν_e from kaon decays.

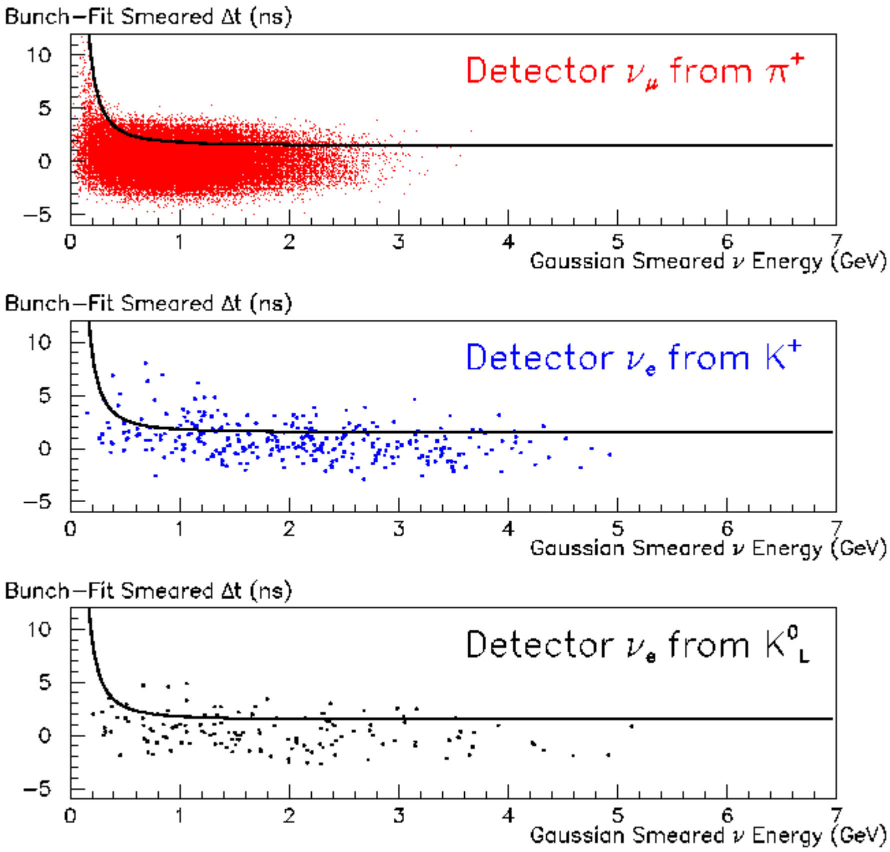

Figure 13: Reconstructed Energy vs. Time of Reconstruction in the detector for parabolic smeared monte carlo data, with the $\Delta t'$ curve overlaid. The reconstructed energy is smeared with a gaussian of width $\sigma_E = \Delta E/E = 0.1$. The time of reconstruction is smeared with the parabolic function derived from the data: $y = 1.605 - 0.331x^2$, see Figure 12, and a gaussian function of $\sigma = 0.9\ ns$ corresponding to the detector timing resolution.

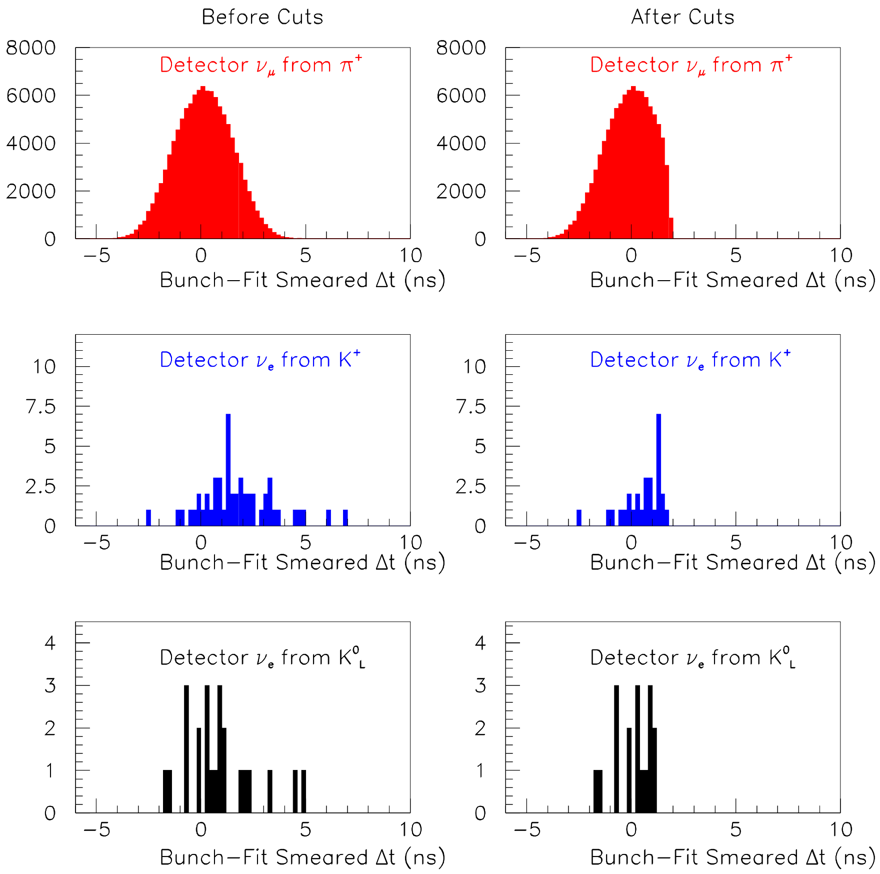

Figure 14: Time of reconstruction distribution for parabolic smeared monte carlo data. The reconstructed energy is smeared with a gaussian of width $\sigma_E = \Delta E/E = 0.1$. The time of reconstruction is smeared with the parabolic function derived from the data: $y = 1.605 - 0.331x^2$, see Figure 12, and a gaussian function of $\sigma = 0.9\ ns$ corresponding to the detector timing resolution.

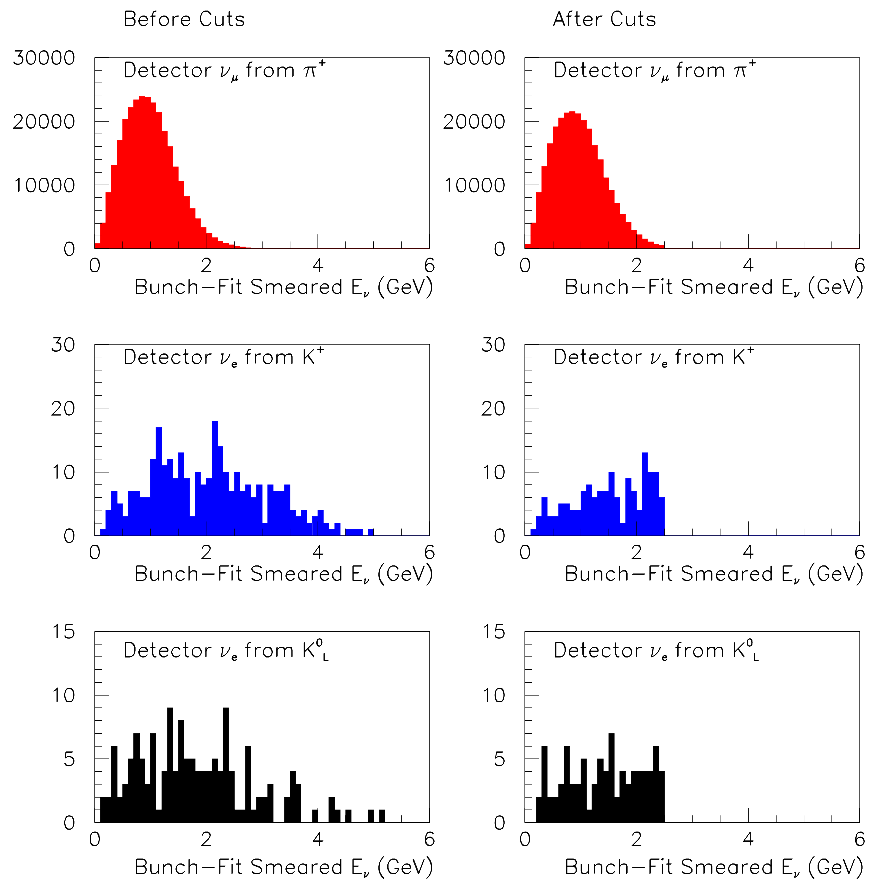

Figure 15: Reconstructed Energy distribution for parabolic smeared monte carlo data. The reconstructed energy is smeared with a gaussian of width $\sigma_E = \Delta E/E = 0.1$. The time of reconstruction is smeared with the parabolic function derived from the data: $y = 1.605 - 0.331x^2$, see Figure 12, and a gaussian function of $\sigma = 0.9\ ns$ corresponding to the detector timing resolution.

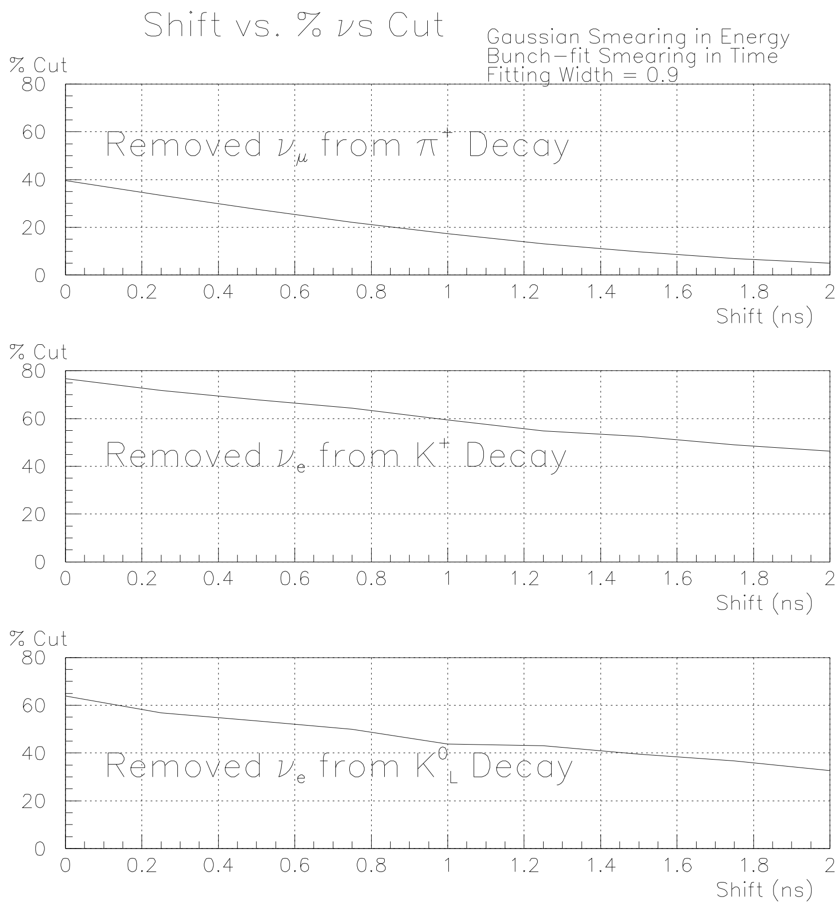

Figure 16: Shift vs. Rejection efficiency for parabolic smeared monte carlo data using $\Delta t < shift + \Delta t_{\nu_\mu,max}$ as a cut. The reconstructed energy is smeared with a gaussian of width $\sigma_E = \Delta E/E = 0.1$. The time of reconstruction is smeared with the parabolic function derived from the data: $y = 1.605 - 0.331x^2$, see Figure 12, and a gaussian function of $\sigma = 0.9\ ns$ corresponding to the detector timing resolution.

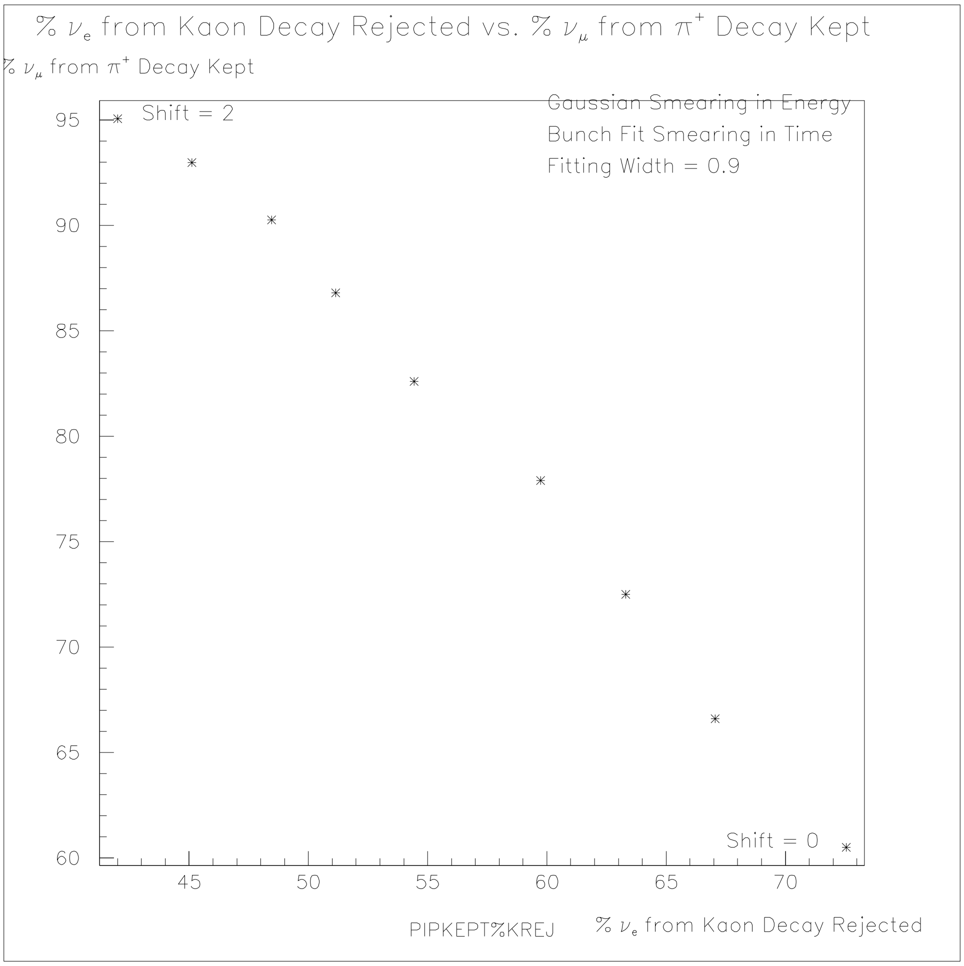

Figure 17: Percent of neutrinos from pion decay retained vs. Percent of neutrinos from kaon decay rejected using $\Delta t' < shift + \Delta t_{\nu_\mu,max}$ as a cut for shift values between zero and two.

4 Conclusions

With realistic smearing in time and reconstructed energy of neutrinos interacting in the detector, we demonstrate an efficiency of $\sim 50\%$ in rejecting electron neutrinos from kaon decays using the difference in time of flight between neutrinos from pions and kaons, with a $\sim 10\%$ loss of muon neutrino flux.

This analysis has been performed using Monte Carlo data produced by GEANT using GFLUKA as the particle generator. Since there are differences between the GFLUKA kaon production model and those of MARS and DPMJET, this analysis will be repeated using the MARS generated flux. A second draft of this memo will be released with the MARS analysis included.